A&A 543, A130 (2012)
DOI: 10.1051/0004-6361/201218869

Astronomy & Astrophysics

VLT and *Suzaku* observations of the *Fermi* pulsar PSR J1028−5819⋆

R. P. Mignani[1,2], M. Razzano[3,4,9], P. Esposito[5], A. De Luca[6,7], M. Marelli[7,8], S. R. Oates[1], and P. Saz-Parkinson[9]

[1] Mullard Space Science Laboratory, University College London, Holmbury St. Mary, Dorking, Surrey, RH5 6NT, UK
e-mail: rm2@mssl.ucl.ac.uk
[2] Kepler Institute of Astronomy, University of Zielona Góra, Lubuska 2, 65-265 Zielona Góra, Poland
[3] Istituto Nazionale di Fisica Nucleare, Sezione di Pisa, 56127 Pisa, Italy
[4] Dipartimento di Fisica "E. Fermi", Università di Pisa, 56127 Pisa, Italy
[5] INAF – Osservatorio Astronomico di Cagliari, località Poggio dei Pini, Strada 54, 09012 Capoterra, Italy
[6] INAF – Istituto di Astrofisica Spaziale e Fisica Cosmica Milano, via E. Bassini 15, 20133 Milano, Italy
[7] INFN – Istituto Nazionale di Fisica Nucleare, sezione di Pavia, via A. Bassi 6, 27100 Pavia, Italy
[8] Università degli Studi dell'Insubria, via Ravasi 2, 21100 Varese, Italy
[9] Santa Cruz Institute for Particle Physics, University of California, Santa Cruz, CA 95064, USA

Received 23 January 2012 / Accepted 18 June 2012

ABSTRACT

Context. The launch of the *Fermi* Gamma-ray Space Telescope in 2008 opened new perspectives in the multi-wavelength studies of neutron stars, with more than 100 γ-ray pulsars having since been detected. While most *Fermi* pulsars had previously been observed in the X-rays with *Chandra* and *XMM-Newton*, optical observations with 8 m-class telescopes exist for only a tiny fraction of them.
Aims. We aim to search for optical emission from the *Fermi* pulsar PSR J1028−5819 (P = 91.4 ms). With a spin-down age $\tau \sim 90$ kyr and a rotational energy loss rate of $\dot{E} \sim 8.3 \times 10^{35}$ erg s^{-1}, PSR J1028−5819 can be considered a transition object between the young, Vela-like pulsars and the middle-aged ones. At a distance of ∼2.3 kpc and with a relatively low hydrogen column density PSR J1028−5819 is a good potential target for 8 m-class telescopes.
Methods. Owing to its recent discovery, no optical observations of this pulsar have been reported so far. We used optical images taken with the Very Large Telescope (VLT) in the B and V bands to search for the optical counterpart of PSR J1028−5819 or constrain its optical brightness. At the same time, we used an archival *Suzaku* observation to confirm the preliminary identification of the pulsar's X-ray counterpart obtained by *Swift*.
Results. Owing to the large uncertainty in the pulsar's radio position and the presence of a bright (V = 13.2) early F-type star at $\lesssim 4''$ (star A), we are unable to detect its counterpart down to flux limits of $B \sim 25.4$ and $V \sim 25.3$, the deepest obtained so far for PSR J1028−5819. From the *Suzaku* observations, we find that the X-ray spectrum of the pulsar's candidate counterpart is best-fit by a power-law with spectral index $\Gamma_X = 1.7 \pm 0.2$ and an absorption column density $N_H < 10^{21}$ cm^{-2}, which would support the proposed X-ray identification. Moreover, we find possible evidence of diffuse emission around the pulsar. If real and associated with a pulsar wind nebula (PWN), its surface brightness and angular extent would be compatible with the expectations for a ∼100 kyr old pulsar at the distance of PSR J1028−5819.
Conclusions. A far more accurate radio position for PSR J1028−5819 is necessary to better determine its position relative to star A. Future high-spatial resolution observations with both the HST and *Chandra* will be more able to distinguish the optical emission of PSR J1028−5819 from the halo of star A and confirm the existence of the candidate PWN.

Key words. stars: neutron – pulsars: individual: PSR J1028–5819 – gamma rays: stars – X-rays: stars

1. Introduction

The launch of NASA's *Fermi* Gamma-ray Space Telescope in June 2008 marked a breakthrough in γ-ray observations of pulsars. The Large Area Telescope (LAT; Atwood et al. 2009) has now detected more than 100 γ-ray pulsars, to be compared with the 7 detected by the *Compton* Gamma Ray Observatory (CGRO) in 10 years of operation (see, e.g. Thompson 2008, for a review). Some of them are associated with known, or recently discovered, radio pulsars, while others are yet undetected in the radio despite some deep searches and are, thus, members of the long-hypothesised class of radio-silent γ-ray pulsars, of which Geminga was the first example (e.g., Bignami & Caraveo 1996; Abdo et al. 2010a). In both cases, multi-wavelength follow-ups are important to study the pulsar radiation processes over several decades in energy, to constrain the source distance and position, and to search for pulsar wind nebulae (PWNe), still challenging targets in γ-rays despite the unprecedented spatial resolution of the *Fermi*-LAT (e.g., Ackermann et al. 2011). In the X-rays, many *Fermi* pulsars had already been observed prior to their γ-ray detection, while for the others systematic follow-up observations have been carried out with *Chandra*, *XMM-Newton*, and *Swift* (see, e.g. Marelli et al. 2011, for a summary of the X-ray observations of *Fermi* pulsars). In the optical, the source coverage with 8 m-class telescopes is still sparse with only a few *Fermi* pulsars having been observed beforehand and only a few deep follow-up observations on well-selected targets

⋆ Based on observations collected at ESO, Paranal, under Programme 086.D-0392(B).

having been carried out so far (Mignani et al. 2011; Shearer et al., in prep.; De Luca et al., in prep.).

The radio pulsar PSR J1028−5819 (P = 91.4 ms) was discovered by Keith et al. (2008) during a 3.1 GHz survey of a sample of low-latitude unidentified EGRET error boxes performed with the Parkes radio telescope and the Australia Telescope Compact Array (ATCA), prior to the launch of *Fermi*. The pulsar's period derivative $\dot{P} = 1.61 \times 10^{-14}$ s s^{-1} yields a spin-down age of ∼90 kyr, a spin-down power $\dot{E} \sim 8.3 \times 10^{35}$ erg s^{-1}, and a dipolar magnetic field $B \sim 1.2 \times 10^{12}$ G. Thus, PSR J1028−5819 may be considered a transition object between the young, Vela-like pulsars and the middle-aged ones. The dispersion measure (DM = 96.525 ± 0.002 cm^{-3} pc) implies a distance of ∼2.3 kpc, according to the Galactic electron-density model of Cordes & Lazio (2002). Initially associated with the EGRET source 3EG 1027−5817 upon its coincidence with the γ-ray error box, PSR J1028−5819 was identified as a γ-ray pulsar by *Fermi* (Abdo et al. 2009a) and included in both the *Fermi* catalogue Bright Source List (Abdo et al. 2009b) and the first *Fermi*-LAT catalogue of γ-ray pulsars (Abdo et al. 2010b). As for many *Fermi* pulsars, the γ-ray light curve is characterised by a double-peak profile, with a phase separation of ∼0.46, which trails the single radio peak by ∼0.2 in phase. The pulsar's γ-ray spectrum is fit by a power law (PL) with an exponential cut-off, a photon index $\Gamma_\gamma = 1.25$, and a cut-off energy $E_c = 1.9$ GeV. Possible evidence of a PWN was also found in the *Fermi* data (Ackermann et al. 2011). Recently, PSR J1028−5819 was found to be spatially coincident with a TeV γ-ray source HESS J1023−575 (Abramowski et al. 2011), whose emission is probably associated with the PWN. In the X-rays, PSR J1028−5819 was identified with a faint X-ray source detected by the *Swift* X-ray Telescope (XRT) in a short follow-up observation (Abdo et al. 2009a; Marelli et al. 2011) of the γ-ray source error box. Unfortunately, the low detection significance ($\lesssim 5\sigma$) hampered the characterisation of the pulsar's X-ray spectrum.

While deeper X-ray observations of PSR J1028−5819 are now in progress with *Chandra*, no optical observations have yet been performed. Here, we present the first optical observations of PSR J1028−5819, performed with the Very Large Telescope (VLT) as a part of a planned survey to optically identify *Fermi* pulsars. To complement our multi-wavelength analysis, we also present a re-analysis of the published *Swift*/XRT observation of the pulsar and the first results of a more recent, yet unpublished, *Suzaku* observation available in the public science data archive.

This paper is organised as follows: observations, data reduction and analysis are described in Sect. 2, while results are presented and discussed in Sects. 3 and 4, respectively. Our conclusions then follow.

2. Observations and data reduction

2.1. VLT observation

PSR J1028−5819 was observed in service mode on February 10 and 11, 2011 with the VLT Antu telescope at the ESO Paranal and the FOcal Reducer/low dispersion Spectrograph (FORS2), which is a multi-mode camera for imaging and long-slit/multi-object spectroscopy (Appenzeller et al. 1998). We used FORS2 used in imaging mode equipped with its standard MIT detector, a mosaic of two 2k × 4k CCDs optimised for wavelengths longer than 6000 Å. With its high-resolution collimator, the detector has a pixel scale of 0.″125 (2 × 2 binning), which corresponds to a projected field-of-view (FOV) of 4.′15 × 4.′15 over the CCD mosaic. However, owing to vignetting, the effective sky coverage is smaller, and is larger for the upper CCD chip.

Observations were performed with the standard low-gain and fast read-out mode, with the high-resolution collimator, and through the high-throughput $b_{\rm HIGH}$ (λ = 4400 Å; $\Delta\lambda$ = 1035 Å) and $v_{\rm HIGH}$ (λ = 5570 Å; $\Delta\lambda$ = 1235 Å) filters. To allow for cosmic ray removal, we obtained sequences of short exposures (100 s) for a total integration time of 4800 s in both the $b_{\rm HIGH}$ and $v_{\rm HIGH}$ filters. We set such a short exposure time to minimise the saturation of a bright V = 13.12 star close to the pulsar position, that had been identified in the Digitised Sky Survey (DSS) images. Exposures were taken in dark time and under photometric conditions, as recorded by the ESO ambient condition monitor[1], with an airmass of ∼1.2 and image quality of ∼0.″8, measured directly on the images by fitting the full-width at half maximum (FWHM) of unsaturated field stars.

Data were reduced through the ESO FORS2 pipeline[2] for bias subtraction and flat-field correction. Per each band, we aligned and average-stacked the reduced science images using the `swarp` programme (Bertin et al. 2002), applying a 3σ filter to the single pixel average to filter out residual hot and cold pixels and cosmic ray hits. Since all exposures were taken with sub-arcsec image quality, we did not perform any selection prior to the image stacking. We applied the photometric calibration by using the extinction-corrected night zero points computed by the FORS2 pipeline, which are available through the instrument data quality control database[3].

2.2. Swift observations

PSR J1028−5819 was pointed by the *Swift*/XRT on November 23rd 2008, during a Target of Opportunity (ToO) observation (Obs ID 00031298001) requested soon after the pulsar detection by *Fermi*. The XRT (Burrows et al. 2005) is a grazing incidence Wolter I telescope equipped with an X-ray CCD imaging spectrometer, yielding a 110 cm^2 effective area at 1.5 keV, a 23.′6 × 23.′6 FOV (2.″36/pixel), and an half energy width of 15″ in the 0.2–10 keV energy range. The integration time was 9.6 ks (7.9 ks accounting for the exposure map correction). The observations were performed in PC mode. Data reduction and analysis were performed as in Marelli et al. (2011) but using the newest version (6.11) of the `HEAsoft` software package[4]. On the same visit, the PSR J1028−5819 field was also observed in the near-UV with the Ultra-Violet Optical Telescope (UVOT) on board *Swift*. The UVOT (Roming et al. 2005) is a 30 cm, f/12.7 Ritchey-Chrétien telescope using a microchannel-intensified CCD detector that operates in photon counting mode, covering the 1600–8000 Å range over a 17′ × 17′ FOV (0.″5/pixel). Observations were performed with the UVM2 (λ = 2246 Å; $\Delta\lambda$ = 498 Å) and the UVW2 (λ = 1928 Å; $\Delta\lambda$ = 657 Å) filters (Poole et al. 2008) for a total integration time of 4115 s and 5701 s, respectively. We retrieved the data from the *Swift* science data archive and combined the single exposures to obtain the best signal-to-noise ratio (S/N). We used the UVOT data analysis software available in `HEAsoft` and the version 20110131 of the UVOT calibration files.

[1] http://archive.eso.org/asm/ambient-server
[2] http://www.eso.org/sci/software/pipelines
[3] www.eso.org/qc
[4] heasarc.gsfc.nasa.gov/docs/software/lheasoft/

2.3. Suzaku observations

The field of PSR J1028–5819 was also observed by *Suzaku* (Mitsuda et al. 2007) on July 22, 2009. The observation (Obs ID 504045010) was performed with the pulsar located at the nominal aim-point position of the X-ray Imaging Spectrometer (XIS; Koyama et al. 2007). The XIS consists of three front-illuminated (FI) CCD cameras (XIS0, XIS2, and XIS3), and one that is back-illuminated (BI; XIS1). Each CCD camera is combined with a single X-ray telescope (Serlemitsos et al. 2007) and has a single chip, yielding a 330 cm^2 (FI) or 370 cm^2 (BI) effective area at 1.5 keV, $18' \times 18'$ field of view ($1\farcs05$/pixel) and a $1\farcm8$ spatial resolution in the 0.2–12 keV energy range. One of the front-illuminated CCDs, XIS2, was unavailable at the time of our observation, since it suffered from a damage on 2006 November 9 and has been unusable since then. The observations were performed in full-frame mode.

We downloaded the data from the public *Suzaku* science data archive through the DARTS interface[5]. Data reduction and analysis of the XIS was performed with `HEAsoft` following the procedures described in the *Suzaku* ABC Guide[6] version 2. We used the task `xispi` to convert the unfiltered XIS event files to pulse-invariant channels and then `xisrepro` to obtain cleaned of event files. For each XIS, both 3×3 and 5×5 edit modes cleaned event data were combined using `xis5x5to3x3` and `xselect`. Following standard practices, we excluded times within 436 s of *Suzaku* passing through the South Atlantic Anomaly and we also excluded the data when the line of sight was elevated above the Earth's limb by less than 5°, or is less than 20° from the bright-Earth terminator. Moreover, we excluded time windows during which the spacecraft was passing through the low cut-off rigidity of below 6 GV. Finally, we removed hot and flickering pixels using `sisclean`. The nominal on-source time is 23 ks. With all the aforementioned data selection criteria applied, the resulting total effective integration time was 20.2 ks. For the spectral analysis, the response matrices were generated with `xisrmfgen` and using ray-tracing simulations with `xissimarfgen`.

3. Results

3.1. VLT astrometry

The radio position of PSR J1028−5819 was obtained through interferometry observations with the ATCA (Keith et al. 2008) and is $\alpha = 10^h28^m27\fs95$ ($\pm0\fs1$) and $\delta = -58°19'05\farcs22$ ($\pm1\farcs5$), at MJD = 54 562. Owing to the relatively small difference of ∼3 yrs between the epoch of the reference radio position and that of our VLT observation, we can neglect any additional uncertainty in the pulsar position due to its unknown proper motion. If we assumed a DM pulsar distance of 2.3 kpc and a transverse velocity three times as large as the peak value of the radio pulsar velocity distribution (∼400 km s^{-1}; Hobbs et al. 2005), the time difference would correspond to an additional uncertainty (in the radial direction) of $\sim0\farcs3$, which is much smaller than the nominal error in the radio position. No more recent (and more accurate) radio position for PSR J1028−5819 has been obtained by the *Fermi* Pulsar Timing Consortium (Smith et al. 2008), with Weltevrede et al. (2010) assuming the original ATCA position of Keith et al. (2008), while the measured *Swift*/XRT position of the pulsar candidate counterpart, $\alpha = 10^h28^m27\fs69$ and $\delta = -58°19'05\farcs16$ (Marelli et al. 2011), has an estimated radial uncertainty of $\sim5''$. Thus, we assume the ATCA radio position as a reference. We note that Simbad reports a quite different position, $\alpha = 10^h28^m39\fs8$ and $\delta = -58°17'31\farcs0$, which is still that given in the *Fermi*-LAT Bright Source List (Abdo et al. 2009b).

To register the pulsar position in the FORS2 frames as precisely as possible, we re-computed their astrometric solution, which is, by default, based on the coordinates of the guide star used for the telescope pointing. As a reference, we used stars selected from the Guide Star Catalogue 2 (GSC-2; Lasker et al. 2008). Although the UCAC-3 catalogue (USNO CCD Astrograph Catalog; Zacharias et al. 2010) has a better astrometric accuracy then the GSC-2, it has a cut-off at brighter magnitudes ($V \lesssim 16$) and most of the reference UCAC-3 stars are saturated even in the short-exposures FORS2 images. We selected GSC-2 stars evenly distributed in the field-of-view but far from the CCD edges and the vignetted regions, where geometric distortions appear to be larger than expected. We noticed this effect for the first time in our data set and, apparently, it affects all FORS2 images taken with the high-resolution collimator after 2009 (van den Ancker, priv. comm.). Its origin is still under investigation. We measured the star centroids by means of Gaussian fitting using the Graphical Astronomy and Image Analysis (GAIA) tool[7] and used the code ASTROM[8] to compute the pixel-to-sky coordinate transformation using an high-order polynomial, which accounts for the CCD distortions. The root mean square (rms) of the astrometric fits was $\sigma_r \sim 0\farcs1$ in the radial direction. To this value, we added in quadrature the uncertainty $\sigma_{tr} = 0\farcs1$ in the registration of the FORS2 image in the GSC2 reference frames, $\sigma_{tr} = \sqrt{(3/N_s)}\sigma_{GSC2}$, where $\sigma_{GSC2} = 0\farcs3$ is the mean positional error of the GSC2 coordinates and N_s is the number of stars used to compute the astrometric solution (Lattanzi et al. 1997). After accounting for the $\sim0\farcs15$ accuracy of the link of the GSC2 coordinates to the International Celestial Reference Frame (ICRF), we thus estimated that the overall (1σ) uncertainty in our FORS2 astrometry is $\delta_r \sim 0\farcs2$. This is negligible compared with the absolute error in the reference pulsar position.

3.2. The search for the pulsar's optical counterpart

The computed PSR J1028−5819 position is shown in Fig. 1, overlaid on the FORS2 V-band image. As mentioned in Sect. 2.1, it falls $\lesssim4''$ from a bright ($V = 13.12$) field star (star A) west of it. Unfortunately, since its halo extends to $\lesssim1''$ from the pulsar position we could not mask star A without the risk of severely hampering our observations. Since the angular separation between star A's halo and the pulsar is indeed compatible with the telescope pointing accuracy and smaller than the absolute uncertainty in the pulsar's position (see above), this could have been accidentally covered by one of the FORS2 occulting bars (∼$12\farcs5$ width with the high-resolution collimator). Moreover, star A is part of a triplet (with star B and C) of relatively bright stars that was not resolved in the DSS-2 images, the only ones available for a quick look of the pulsar field, owing to their coarse spatial resolution. This would have caused the mask to be put even closer to the pulsar position, thus increasing the risk of an accidental occultation of our target. We note that the northern star of the triplet (star B) overlaps the pulsar position. However, its relatively high flux ($B \sim 20.3 \pm 0.1$; $V \sim 17.5 \pm 0.1$) obviously rules it out as a possible candidate counterpart to the pulsar (e.g., Mignani 2011). The same argument also applies to

[5] `www.darts.isas.jaxa.jp/astro/suzaku/`
[6] `heasarc.gsfc.nasa.gov/docs/suzaku/analysis/abc/`
[7] `star-www.dur.ac.uk/~pdraper/gaia/gaia.html`
[8] `www.starlink.rl.ac.uk/star/docs/sun5.htx/sun5.html`

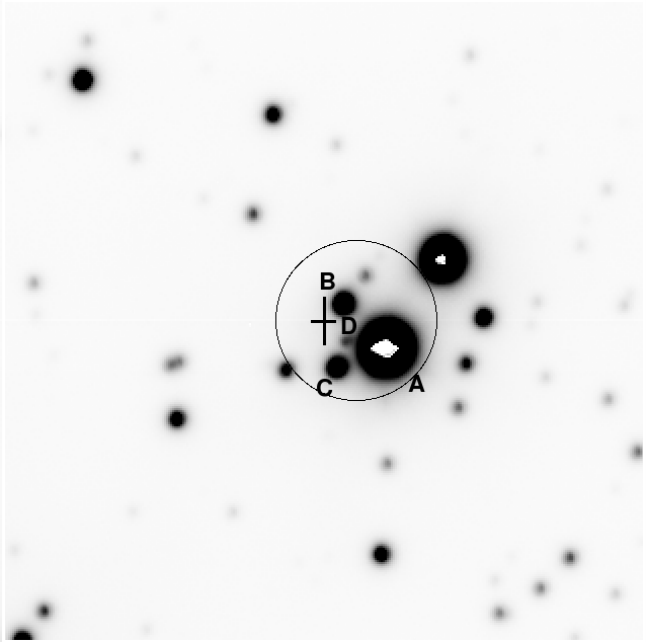

Fig. 1. The 40″ × 40″ VLT/FORS2 image of PSR J1028−5819 in the $v_{\rm HIGH}$ filter (4800 s). North to the top, east to the left. The cross marks the pulsar radio-interferometry position (Keith et al. 2008), while the circle (∼5″ radius) marks the position of the candidate X-ray counterpart detected by *Swift*/XRT (Abdo et al. 2009a; Marelli et al. 2011). Stars close to the radio position are labelled (A–D). The bright star A (V = 13.12) is saturated in the FORS2 image. The intensity scale in the image has been stretched to help visualise the fainter stars (B–D).

the southern star of the triplet (star C), which is of comparable brightness ($B = 20.7 \pm 0.1$; $V \sim 17.5 \pm 0.1$).

A fourth, fainter star (star D) is visible in the V-band image at ∼2″ from the nominal radio pulsar position, superimposed on the halo of the much brighter star A, while in the B-band image it cannot be clearly resolved, partially because of the slightly poorer image quality. The offset is comparable with the 1σ uncertainty in the pulsar position, which, in principle, makes it a possible candidate counterpart. We computed the flux of star D through customised aperture photometry using a small aperture of four pixel radius (0.″5) to minimise the contribution of the bright star A's halo and optimise the S/N. We sampled the local background within circular areas of the same radius as the photometry aperture placed below and above the star D's position. We then computed the aperture correction using the growth curves of a few unsaturated field stars. The computed magnitudes are $B \sim 22.5 \pm 0.2$ and $V \sim 20.5 \pm 0.2$, where the photometric errors are dominated by the uncertainty in the subtraction of the background of the bright star A's halo, which also makes it an improbable candidate pulsar counterpart.

The positions and fluxes of all stars detected close to the PSR J1028−5819 position are summarised in Table 1. No other object is clearly visible at, or close to, the radio pulsar position. Although our images were taken under sub-arcsec seeing conditions and with short exposure times to minimise the flux contamination of star A, its bright halo still significantly affects the background close to the pulsar position, hampering the detection of its faint counterpart. We tried to subtract star A using the model image point spread function (PSF), computed by fitting the intensity profile of several unsaturated field stars. To this aim, we used the tools `daofind`, `nstar`, `peak`, and `substar` available in the IRAF package `daophot`. Since star A is partially saturated, this procedure obviously leaves some residuals at the PSF core, but can account for the subtraction of most of the PSF and its wings. Similarly, we also PSF-subtracted the stars B, C, and D.

Table 1. Coordinates and fluxes of the stars detected close to the PSR J1028−5819 position (see Fig. 1).

Star	α ($^{\rm h\,m\,s}$)	δ ($^\circ\ '\ ''$)	B	V
A	10 28 27.472	–58 19 06.92	12.9 ± 0.1	13.1 ± 0.1
B	10 28 27.764	–58 19 04.22	20.3 ± 0.1	17.5 ± 0.1
C	10 28 27.819	–58 19 08.19	20.7 ± 0.1	17.5 ± 0.1
D	10 28 27.741	–58 19 06.56	22.5 ± 0.3	20.5 ± 0.2

Notes. For star A, which is saturated in the FORS2 image, we list the GSC-2 magnitudes and assume the photometric accuracy given in the catalogue (Lasker et al. 2008). The flux uncertainties for stars B–D accounts for both statistical errors and the absolute accuracy of the FORS2 photometric calibration. The absolute accuracy of the star positions is $\delta_{\rm r} \sim 0.''2$, as given by our astrometry calibration (see Sect. 3.1).

We did not detect any excess signal in the PSF-subtracted images, which can be associated with emission from a point-like source at the pulsar position. Thus, we concluded that PSR J1028−5819 was not detected in our VLT images. We computed the optical flux upper limits in the PSF-subtracted B and V bands images from the rms of the background sampled in the pulsar radio error box within cells of 7 × 7 pixels, i.e. of size equal to the computed image FWHM, and we applied the computed aperture correction. We then derived 3σ upper limits of $V \sim 25.3$ and $B \sim 25.4$. Unfortunately, these limits are affected by the residuals of the PSF subtraction of the four stars, to which star A and B are contributing the most, and which increase the local sky background by a factor of four with respect to other regions in the field, where the limiting magnitudes are about 1.5 mag deeper.

3.3. The pulsar's X-ray counterpart: Swift observation

It is interesting to compare our derived optical flux upper limits on PSR J1028−5819, the deepest obtained so far, with the extrapolation of the best-fit to the X-ray spectrum of the pulsar's counterpart. Unfortunately, this is poorly constrained by the available *Swift*/XRT observation (Fig. 2), owing to the short integration time (7.9 ks) and the low count statistics. We extracted all counts within a 20″ radius using a similarly sized background region. This yields $(2.41 \pm 0.69) \times 10^{-3}$ counts s^{-1} in the 0.3–10 keV energy range. We reanalysed the XRT spectral data using the newest version (12.7) of the XSPEC fitting package (Arnaud et al. 1996). As in Marelli et al. (2011), we found a satisfactory fit with a PL of fixed photon index $\Gamma_{\rm X} = 2$, assuming a fixed hydrogen column-density $N_{\rm H} \sim 5 \times 10^{21}$ cm^{-2} inferred from the Galactic value along the line of sight using the `Heasarc nH` tool[9] scaled to the pulsar distance of 2.3 kpc assuming a constant distribution. We note that this value of the $N_{\rm H}$ is about a factor of three lower than assumed by Abdo et al. (2009a), $N_{\rm H} = 1.59 \times 10^{22}$ cm^{-2}, whose determination, however, is not explained. For these spectral parameters, the *Swift*/XRT spectrum corresponds to an unabsorbed 0.5–10 keV X-ray flux $F_{\rm X} = (1.5 \pm 0.5) \times 10^{-13}$ erg cm^{-2} s^{-1}.

[9] http://heasarc.gsfc.nasa.gov/cgi-bin/Tools/w3nh/w3nh.pl

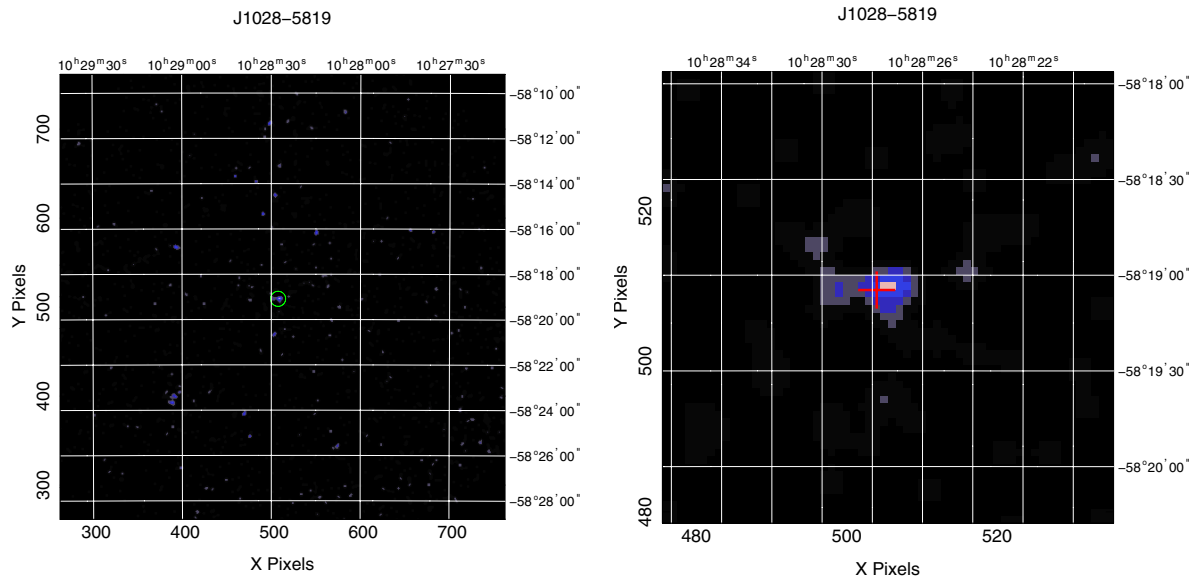

Fig. 2. *Left panel*: *Swift*/XRT image (20′ × 20′) of the field of PSR J1028–5819 in the 0.3–10 keV energy range. The source highlighted by the green circle is the pulsar's X-ray counterpart (Abdo et al. 2009a; Marelli et al. 2011). *Right panel*: zoom-in of the *Swift*/XRT image (2.′5 × 2.′5) on the source position. The red cross marks the ATCA position of PSR J1028–5819 (Keith et al. 2008).

3.4. The pulsar's X-ray identification revisited

The uncertainty in the pulsar's X-ray spectrum obviously affects the comparison with our optical flux measurements. Moreover, the positional coincidence between the *Swift*/XRT error circle of the pulsar candidate counterpart and star A (Fig. 1) suggests that, in principle, this might contribute to the observed X-ray emission, which would make the characterisation of the pulsar X-ray spectrum even more uncertain. As a most extreme possibility, it cannot be ruled out that the *Swift*/XRT source is, actually, the X-ray counterpart to star A and not to the pulsar. The star was clearly detected by the *Swift*/UVOT (see Fig. 3) but, admittedly, its possible contribution to the emission of the X-ray source was not accounted for by Marelli et al. (2011). Thus, we tried to evaluate such a contribution by determining the star's spectral type via multi-band photometry.

For the *Swift*/UVOT observations, we used the FTOOL `uvotsource` to determine the count rate of the star in both the UVM2 and UVW2 filters. We used a 2″ aperture to minimise the contamination from the nearby star north-west of it. The count rate was aperture-corrected to a radius of 5″ to apply the count-rate to magnitude conversion using the zero pointsof the *Swift*/UVOT calibration (Breeveld et al. 2010, 2011). The computed magnitudes (in the Vega system) are $m_{\rm UVM2} = 16.29 \pm 0.10$ and $m_{\rm UVW2} = 16.51 \pm 0.11$, where the associated errors are purely statistical (systematic errors are ∼0.03 mag). The star's optical magnitudes are $R_{\rm F} = 12.87$ and $V = 13.12$, according to the GSC-2 (Lasker et al. 2008), while the near-infrared magnitudes, derived from 2MASS (Skrutskie et al. 2006), are $J = 12.38$, $H = 12.16$, and $K_{\rm s} = 12.09$. Unfortunately, the UVOT, DSS, and 2MASS, images have insufficient angular resolution to resolve the triplet of stars around star A, while the star ≈7″ north-west of it (Fig. 1) is clearly resolved in all of them (see, e.g. Fig. 3). Thus, the above magnitudes must be interpreted with due care. However, from our VLT data we see that star B and C are at least a factor of ∼50 fainter than star A in both the *B* and *V* bands. Thus, their contribution only marginally affects the estimate of the star colours.

The colours of star A are compatible with those of an early F-type main-sequence star, assuming an interstellar extinction

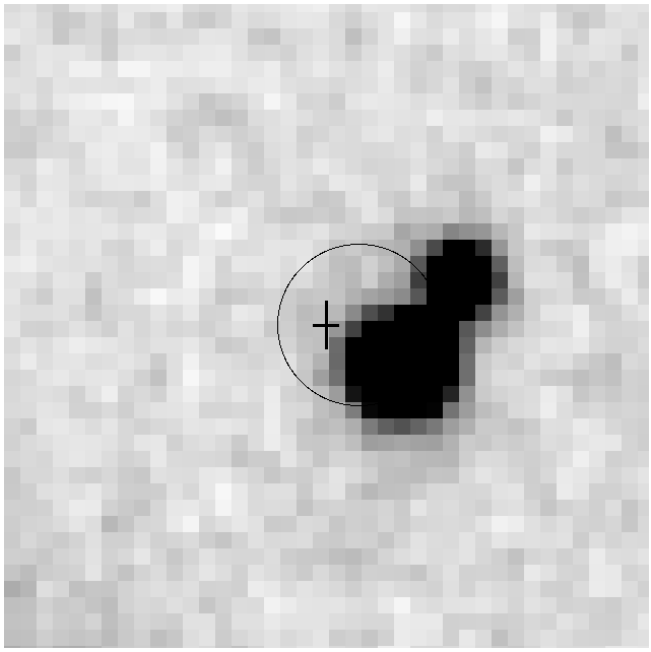

Fig. 3. Same field as in Fig. 1 (40″ × 40″) but obtained by the *Swift*/UVOT through the UVM2 filter (4115 s). North to the top, east to the left. The group of stars around star A (see Fig. 1) is unresolved at the UVOT spatial resolution.

corresponding to an $E(B-V) \sim 0.09$. According to the relation of Predhel & Schmitt (1995), this value would correspond to an $N_{\rm H} \sim 0.5 \times 10^{21}$ cm^{-2}, i.e. lower than estimated by scaling the Galactic value along the line of sight for the PSR J1028−5819 distance, suggesting that star A is, possibly, in the foreground to the pulsar, which would be consistent with a distance of ≈1 kpc derived from its distance modulus. Usually, F-type stars have an X-ray-to-optical flux ratio $F_{\rm X}/F_{\rm V} \approx 10^{-3}$–$10^{-2}$ (e.g. Krautter et al. 1999), which might yield an X-ray flux comparable with that of the *Swift*/XRT source. Thus, it is possible that this is, indeed, the X-ray counterpart to Star A and not to the pulsar.

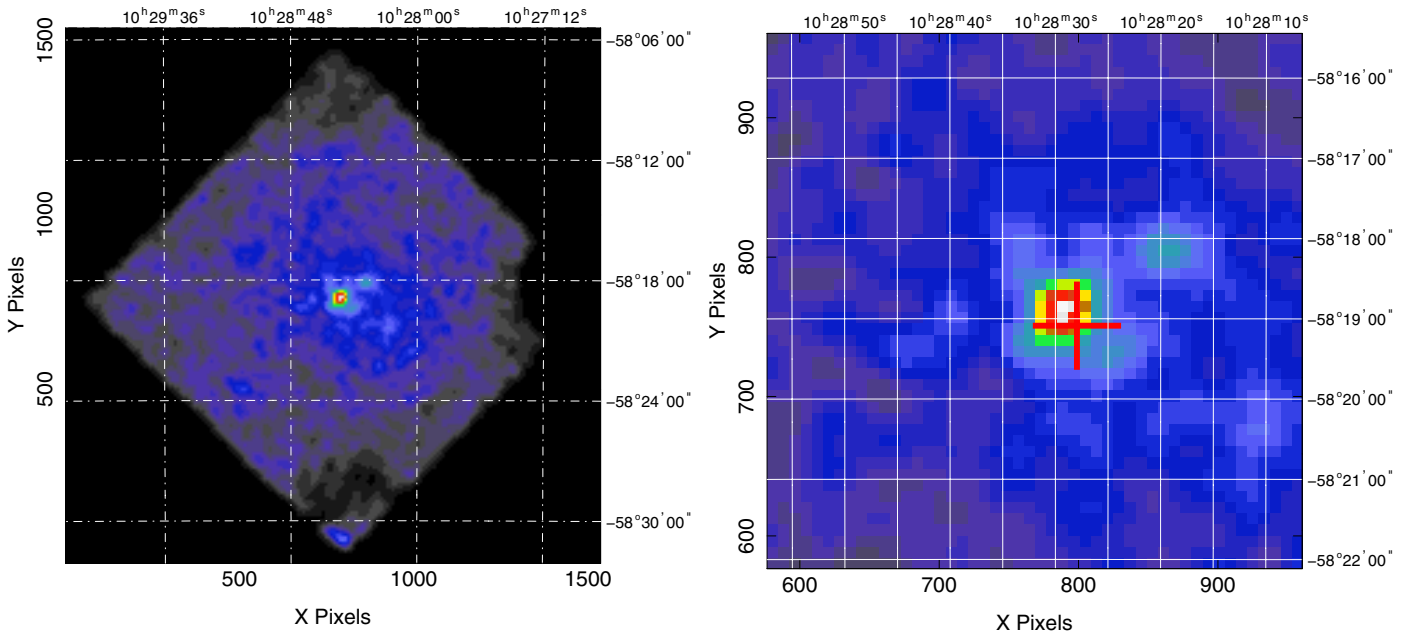

Fig. 4. *Left panel*: *Suzaku*/XIS image ($25' \times 25'$) of the field of PSR J1028–5819 in the 0.2–10 keV energy range. The pulsar's X-ray counterpart, also detected by the *Swift*/XRT (Abdo et al. 2009a; Marelli et al. 2011; Fig. 2), is at the centre of the field-of-view. *Right panel*: zoom-in of the *Suzaku*/XIS image ($6\farcm5 \times 6\farcm5$) at the source position. As in Fig. 2, the red cross marks the ATCA position of PSR J1028–5819 (Keith et al. 2008).

However, any conclusion may still be altered by a more accurate characterisation of the X-ray source spectrum and flux. To achieve this aim, we used an archival *Suzaku* observation (see Sect. 2.3).

3.5. The pulsar's X-ray counterpart: Suzaku observation

The *Suzaku* image of the PSR J1028–5819 field obtained combining the data from the three XIS cameras is shown in Fig. 4. Using the sliding-cells source detection algorithm in the `ximage` package, a source is detected at the centre of the XIS FOV with a S/N of 18 in the 0.2–10 keV energy range. The source best-fit position, $\alpha = 10^{\rm h}28^{\rm m}28\fs7$, $\delta = -58°18'59\farcs3$ (J2000), is consistent, within the absolute astrometry accuracy of *Suzaku* ($\sim 20''$; Uchiyama et al. 2008), with both the ATCA coordinates of PSR J1028–5819 and the coordinates of the source detected by *Swift*.

We extracted the source counts from each XIS detector using a circular region of $0\farcm7$ radius centred on the best-fit `ximage` position. This comparatively small region, corresponding to ~50% of the encircled energy fraction, was chosen to improve the S/N of the spectra and reduce the possible contamination from the diffuse emission apparent in Fig. 4. The background was extracted from annuli with radii $3'$ and $5'$ centred on the X-ray source. Accounting for the counts of all the XIS detectors, the 0.5–10 keV net source count rate is $(2.7 \pm 0.3) \times 10^{-3}$ counts s^{-1}, which is not a very reliable statistical measurement for a detailed spectral analysis. To increase the quality of the photon statistics, we merged the source spectral files and response matrices using `addascaspec`. The 3-XIS spectrum was binned so that each bin contained a minimum of 15 counts. As done for the *Swift*/XRT spectrum, we performed our spectral fits using the `XSPEC` fitting package (version 12.7). The fit to an absorbed PL model (Fig. 5) yields a spectral index $\Gamma_{\rm X} = 1.7 \pm 0.2$ and an absorption that is poorly constrained at $N_{\rm H} < 10^{21}$ cm^{-2} at (1σ), with a reduced $\chi^2_\nu = 1.09$ for 21 degrees of freedom. This corresponds to an unabsorbed 0.5–10 keV X-ray flux $F_{\rm X} = (1.5 \pm 0.2) \times 10^{-13}$ erg cm^{-2} s^{-1}, which is strongly consistent with the value

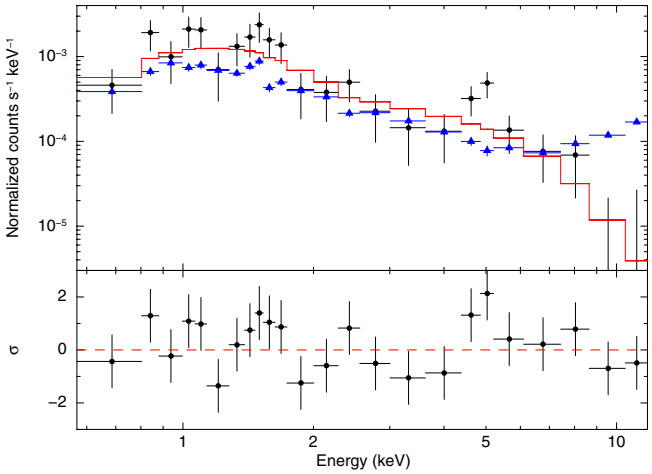

Fig. 5. *Upper panel*: *Suzaku*/XIS spectrum of the candidate PSR J1028−5819 X-ray counterpart obtained using data from the three XIS CCDs. The background level is marked in blue and the best-fit PL model in red. *Lower panel*: fit residuals. The residuals show some (rather small) structures. In the 1.5–2 keV interval, they are probably associated with the Si K-edge remain, while around 5 keV they likely arise from the different responses of the BI and FI detectors around this energy. However, we note that most residuals are within 1σ from the best-fit PL model.

derived by Marelli et al. (2011) from the *Swift*/XRT observation across a similar energy range. We note that our upper limit to the $N_{\rm H}$ is lower than the value inferred by scaling the Galactic value along the line of sight (Marelli et al. 2011), although it is not incompatible with the latter once the associated uncertainties are taken into account. We also tried other single-component models, such as a blackbody (BB), a bremsstrahlung, and a Raymond-Smith plasma (Raymond & Smith 1977). However, they all give higher χ^2 values than the PL, although the fits obtained using the bremsstrahlung and Raymond-Smith plasma models are only slightly worse than obtained using the PL (see

Table 2. Summary of the *Suzaku*/XIS spectral analysis.

Model	$N_{\rm H}$ (10^{21} cm^{-2})	$\Gamma_{\rm X}$	kT (keV)	Observed/unabsorbed flux[a] (10^{-13} erg cm^{-2} s^{-1})		χ^2_ν/d.o.f.
Power law	<1	1.7 ± 0.2	–	$1.5^{+0.1}_{-0.4}$	1.5 ± 0.2	1.09/21
Bremmstrahlung	<0.5	–	8^{+12}_{-3}	$1.4^{+0.1}_{-0.5}$	1.4 ± 0.2	1.16/21
Raymond-Smith	<0.6	–	7^{+10}_{-3}	$1.4^{+0.1}_{-0.4}$	$1.5^{+0.1}_{-0.3}$	1.17/21
Blackbody	<0.5	–	0.5 ± 0.1	0.7 ± 0.2	0.7 ± 0.1	1.97/21

Notes. Errors are at a 1σ confidence level for a single parameter of interest. [(a)] In the 0.5–10 keV energy range.

Table 2 for a summary). To improve our results, we tried to fit the joint *Swift*/XRT and *Suzaku*/XIS spectra, but owing to the low quality statistics of the former observation our results did not change significantly.

Our spectral fits confirm the qualitative results of Marelli et al. (2011), which were based on a lower quality statistics. In particular, the good fit with a PL (χ^2_ν = 1.09) suggests that the spectrum of the X-ray source is non-thermal. Thus, it would not be produced by coronal emission from a main-sequence star, such as Star A. This would confirm that the X-ray source detected by both the *Swift*/XRT and *Suzaku* is, indeed, the pulsar's X-ray counterpart. Owing to the still limited quality of the statistics, we were unable to attempt spectral fits with two-component models, such as a PL+BB. Thus, we cannot rule out that star A might, indeed, contribute at some level to the observed X-ray emission. Deeper observations with *XMM-Newton* will allow one to obtain a more precise characterisation of the X-ray spectrum of the PSR J1028−5819 counterpart, while optical spectroscopy of star A will provide a far more precise classification of its spectral type, allowing one to better quantify its expected X-ray flux. In addition, high-resolution *Chandra* images will allow one to spatially resolve a possible X-ray source associated with star A from the pulsar's X-ray counterpart and secure its identification through the detection of X-ray pulsations[10].

We also inspected the *Suzaku* data to search for possible evidence of a PWN associated with PSR J1028−5819. As mentioned above, diffuse emission on a scale of a few arcminutes is observed around the pulsar's X-ray counterpart (Fig. 4), with an apparent elongation in the south-west direction. The count rate in this region is (5.3 ± 0.5) × 10^{-4} counts s^{-1} arcmin^{-2} in the 0.2–10 keV energy range, computed after summing the counts collected with the three XIS detectors. However, since each XRT/XIS detector has a different position-dependent and broad PSF, with a complicated (roughly cross-shaped) and asymmetric profile (see, e.g. Sugizaki et al. 2009), it is difficult to determine whether the diffuse emission observed around the pulsar's X-ray counterpart is real. As a test, we compared its surface brightness profile with that of a reference X-ray source. Since no suitable sources were detected in the PSR J1028−5819 field-of-view (Fig. 4), we used as a reference an X-ray source detected in another *Suzaku* observation (Obs ID 804017020) and identified this with the ms-pulsar PSR J1231−1411. Since both sources were observed on-axis, our comparison is unaffected by the position dependance of the XIS PSF. In both cases, we selected photons in the 0.3–10 keV energy range in all the three XIS detectors and used the `xissim` tool to simulate and subtract the background, accounting for the detector vignetting.

[10] We note that the frame times of the *Swift*/XRT in PC mode and the *Suzaku*/XIS in full-frame mode are 2.507 s and 8 s, respectively, which makes it impossible to search for pulsations at the PSR J1028−5819 91.4 ms period.

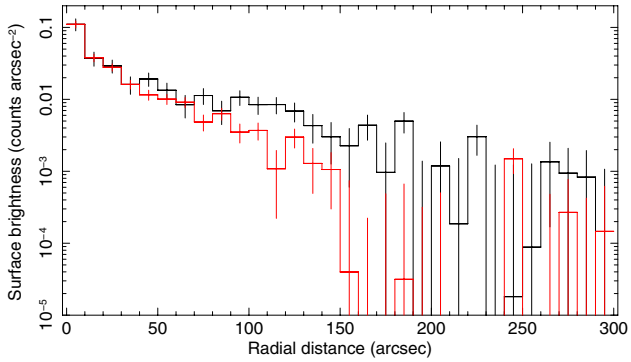

Fig. 6. Surface brightness profiles of the PSR J1028−5819 X-ray counterpart (black) detected in the *Suzaku*/XIS data and of a reference X-ray source (red). The excess with respect to the reference source differs from zero at the ∼5σ level (accounting for statistical errors only). This suggests that diffuse X-ray emission surrounds PSR J1028−5819 on angular scales of a few arcminutes.

Then, we extracted the radial intensity profiles, averaged over a 360° angle, for both the PSR J1028−5819 counterpart and the reference source. Finally, we normalised the counts of the reference source, computed within a radial distance bin of 10″, to that of the PSR J1028−5819 counterpart. As seen from Fig. 6, the latter seems to display an excess of counts with respect to the reference X-ray source at radial distances ∼80″–200″, although this excess is much less evident at larger distances. This, coupled with the low count-rate of the diffuse emission, makes it difficult to determine whether the source detection is real, hence possibly associated with either a PWN or an unresolved field source, and to quantify its contribution to the observed emission of the PSR J1028−5819 X-ray counterpart, in particular at angular distances smaller than 80″. *Chandra* observations will be crucial to confirm the presence of the diffuse emission observed by *Suzaku*. If the source is real, future measurements of the PSR J1028−5819 radio proper motion will, then, allow one to search for its possible alignment with the semi-major axis of the candidate PWN.

4. Discussion

4.1. The pulsar luminosity

We used our magnitude upper limits in the B-band[11] to compute the corresponding extinction-corrected optical flux and luminosity of PSR J1028−5819. As a reference for the interstellar extinction correction, we assumed the upper limit to the hydrogen column density ($N_{\rm H}$ = 10^{21} cm^{-2}) derived from the

[11] For comparison with the luminosities quoted in Zharikov et al. (2006), which are computed in the B band.

fits to the *Suzaku* X-ray spectrum. According to the relation of Predhel & Schmitt (1995), this corresponds to an interstellar extinction $A_V \sim 0.55$. Using the extinction coefficients of Fitzpatrick (1999), the extinction-corrected B-band upper limit is, thus, $F_B \lesssim 9 \times 10^{-16}$ erg cm^{-2} s^{-1}. If we assumed for the pulsar the unabsorbed *Suzaku* X-ray flux derived from the best-fit PL model, $F_X = (1.5 \pm 0.2) \times 10^{-13}$ erg cm^{-2} s^{-1}, our extinction-corrected B-band upper limit would correspond to an X-ray-to-optical flux ratio $F_X/F_B \gtrsim 150$, which is too low to independently suggest that the X-ray source detected by *Swift* and *Suzaku* is indeed the PSR J1028−5819 counterpart. We computed the upper limit to the pulsar optical luminosity using as a reference its DM-based distance of ∼2.3 kpc (Keith et al. 2008). We note that while the uncertainty in the measured DM is negligible (DM = 96.525 ± 0.002 cm^{-3} pc), the Galactic electron density model of Cordes & Lazio (2002) is known to have an average uncertainty of ∼30%, which, however, can be much larger for individual objects. As in the first *Fermi*-LAT catalogue of γ-ray pulsars (Abdo et al. 2010a), we assumed the typical 30% uncertainty on the nominal DM-based distance of PSR J1028−5819. This corresponds to an uncertainty of 0.7 kpc, which we assume in the following discussion. The B-band flux upper limit corresponds to an optical luminosity $L_B \lesssim 9.2 \times 10^{29}$ erg s^{-1} for PSR J1028−5819, after accounting for the assumed distance uncertainty. Given the pulsar spin-down age of ∼90 kyr, we can assume that its, yet undetected, optical emission be purely non-thermal, as normally observed in the youngest pulsars (see, e.g. Mignani 2011). Thus, for the pulsar's spin-down power, $\dot{E} \sim 8.43 \times 10^{35}$ erg s^{-1}, our luminosity upper limit implies an optical emission efficiency $\eta_B \equiv L_B/\dot{E} \lesssim 1.09 \times 10^{-6}$. Both limits are consistent with the optical luminosity and efficiency computed for most pulsars older than ∼0.1 Myr (Zharikov et al. 2006) and confirm an apparent turnover in the pulsar optical-emission properties. Similarly, the pulsar X-ray flux derived from the best-fit PL mode would correspond to an X-ray luminosity $L_X = (9.5 \pm 5.9) \times 10^{31}$ erg s^{-1}, after accounting for the X-ray flux and pulsar distance uncertainties. This value would imply an X-ray emission efficiency $\eta_X \equiv L_X/\dot{E} = (1.13 \pm 0.70) \times 10^{-4}$, for an assumed beaming factor $f = 1$. The derived X-ray efficiency would be consistent, within the large scatter, with the trend observed for the *Fermi* pulsars (Marelli et al. 2011).

4.2. The pulsar multi-wavelength spectrum

We compared the extinction-corrected B and V-band spectral flux upper limits with the extrapolations in the optical domain of the X-ray and γ-ray spectra of PSR J1028−5819. For the X-ray spectrum, we used as a reference our best-fit PL model with spectral index $\Gamma_X = 1.7 \pm 0.2$, while for the γ-ray spectrum we assumed a PL with exponential cutoff, spectral index $\Gamma_\gamma = 1.25 \pm 0.17$, and cutoff energy $E_c = 1.9 \pm 0.5$ GeV, obtained from a reanalysis of the *Fermi* data (see also Marelli et al. 2011). The multi-wavelength spectral energy distribution (SED) of PSR J1028−5819 is shown in Fig. 7, where we accounted for the 1σ uncertainty in the extrapolations of the X and γ-ray PL spectra. The optical spectral flux upper limits are clearly above the extrapolation of the γ-ray PL, which does not rule out the optical emission of PSR J1028−5819 being associated with the low-energy tail of the γ-ray spectrum, as suggested for most γ-ray pulsars identified in the optical (Durant et al. 2011). This would imply that there is a break in the optical-to-X-ray spectrum, as observed in most pulsars (see, e.g. Mignani et al. 2010). In this case, the observed optical flux would be $B = 28$−34,

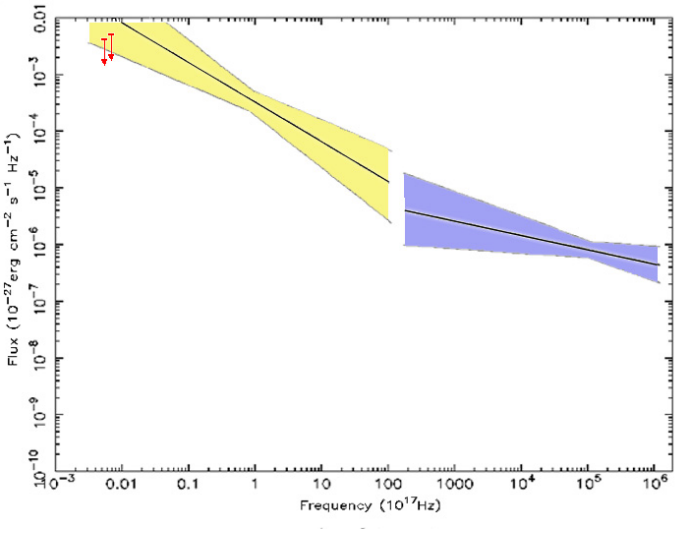

Fig. 7. Upper limits to the extinction-corrected optical fluxes of PSR J1028−5819 compared with the low-energy extrapolations of the X-ray and γ-ray PLs that most closely fits the *Suzaku* and *Fermi* (Abdo et al. 2009a) data (black solid lines). The yellow and blue-shaded areas indicate the 1σ uncertainty in the extrapolations of the X and γ-ray PLs, respectively. The plotted optical flux upper limits are corrected for interstellar extinction based upon an $N_H = 10^{21}$ cm^{-2}.

a range only marginally reachable by current 8 m-class telescopes. On the other hand, the optical upper limits are also compatible with the extrapolation of the X-ray PL, which does not allow one yet to confirm the presence of a possible spectral break in the optical-to-X-ray spectrum. In general, the SED suggests that no single PL can fit the optical-to-γ-ray spectrum of the pulsar, with at least one spectral break required between the X and γ-ray energy ranges. This trend has also been observed in other *Fermi* pulsars (e.g., Mignani et al. 2011), and probably related to complex particle energy and density distributions in the neutron star magnetosphere.

4.3. The candidate PWN

Finally, we verified whether the diffuse emission marginally detected in the *Suzaku* data (Sect. 3.5) would be compatible, if it were indeed a PWN, with the PSR J1028−5819 energetics and distance. PWNe have been detected in the X-rays around a number of young and energetic pulsars (see, e.g. Kargaltsev & Pavlov 2010, for a recent compilation), with luminosities equal to $\sim 10^{-4}$–10^{-2} of the pulsar spin-down power $\dot{E}$. In the case of PSR J1028−5819, one would then expect an X-ray luminosity $L_{X,PWN} \sim 8.5 \times 10^{31}$ erg s^{-1} for its PWN, assuming $L_{X,PWN}/\dot{E} = 10^{-4}$. At the PSR J1028−5819 distance of $\sim 2.3 \pm 0.7$ kpc, this would correspond to an integrated flux of $F_{X,PWN} \sim (1.3 \pm 0.8) \times 10^{-13}$ erg cm^{-2} s^{-1} for the PWN. By using the `WebPIMMS` tool[12] assuming a PWN spectral index $\Gamma_{X,PWN} = 2$ and a hydrogen column density $N_H \sim 10^{21}$ cm^{-2}, this would correspond to a count-rate of $(8 \pm 5) \times 10^{-3}$ counts s^{-1} in the 0.2–10 keV energy range. Following, for instance Bamba et al. (2010), a PWN around a ∼100 kyr old pulsar would have an angular extent of ∼11.″5–21.″5 at a distance of 2.3 ± 0.7 kpc, i.e. comparable to that of the diffuse emission detected in the *Suzaku* data. For the expected PWN extension, we would then derive an expected count rate of $\sim (0.2$–$3) \times 10^{-5}$ counts s^{-1} arcmin^{-2}. This

[12] http://heasarc.nasa.gov/Tools/w3pimms.html

value is up to a factor of 30 lower than the actual count-rate measured for the diffuse emission around PSR J1028−5819. However, it is not incompatible with it if one assumes, e.g. either a correspondingly larger $L_{\rm X,PWN}/\dot{E}$, which would still be within the observed range for the known PWNe, or a non-uniform PWN surface brightness. Thus, it is indeed plausible that the diffuse emission detected by *Suzaku* is associated with the PSR J1028−5819 PWN.

5. Summary and conclusions

We have performed the first deep observations of the *Fermi* pulsar PSR J1028−5819 with the VLT. Unfortunately, owing to a bright star F-type star (star A; $V = 13.12$) ∼4″ away from the pulsar radio position (Keith et al. 2008) we could only set limits of $V \sim 25.3$ and $B \sim 25.4$ on its optical flux, which are admittedly affected by both the residuals after the subtraction of star A's PSF and the coarse accuracy of the radio coordinates. These limits correspond to an optical luminosity $L_B \lesssim 9.2 \times 10^{29}$ erg s^{-1} and emission efficiency $\eta_B \lesssim 1.09 \times 10^{-6}$, which are consistent with the pulsar spin-down age of ∼90 kyr. We have also analysed archival *Suzaku* observations of PSR J1028−5819, which provide a more secure detection of the pulsar's X-ray candidate counterpart and support its identification as a pulsar based on a more accurate characterisation of the X-ray spectrum, which is best-fit by a PL with spectral index $\Gamma_{\rm X} = 1.7 \pm 0.2$. The inferred pulsar's X-ray efficiency ($\eta_{\rm X} \sim 1.13 \times 10^{-4}$) would be consistent with the trend observed for the *Fermi* pulsars (Marelli et al. 2011). The pulsar multi-wavelength spectrum cannot be fit by a single PL, implying that there is at least one spectral break in the optical-to-γ-ray energy range, as observed in other *Fermi* pulsars. We have also found tentative evidence of X-ray diffuse emission around PSR J1028−5819, with a surface brightness and angular extent consistent with the observed X-ray luminosity and size of known PWNe. More observations are required to complete the multi-wavelength study of PSR J1028−5819 at low energies. On the optical side, high-spatial resolution observations with the HST, possibly in the near-UV to exploit the low interstellar extinction along the line of sight, that would be coupled with a much more accurate radio position, are needed to resolve the pulsar emission against the PSF wings of star A. Moreover, optical spectroscopy of star A is needed to provide a more precise classification of its spectral type, allowing one to more accurately predict its X-ray flux. On the X-ray side, follow-up observations with *XMM-Newton* and *Chandra* are needed to obtain a more accurate characterisation of the pulsar's X-ray spectrum, accounting for any possible contribution from star A, and detect X-ray pulsations, which will confirm the proposed identification. *Chandra* observations will also be crucial in confirming the existence of the diffuse emission marginally detected by *Suzaku* and study its spectrum and morphology.

Acknowledgements. A key contributor to the FORS2 pipeline, Carlo Izzo (ESO), prematurely passed away on June 23, 2011 after fighting courageously a short illness. Thanks to Carlo's work, the results from many FORS2 observations were published, making his legacy forever lasting. R.P.M. thanks Paul Ray for checking the PSR J1028−5819 coordinates and Mario van den Ancker and Sabine Moheler (ESO) for investigating the FORS2 geometric distortions. The authors thank Fabio Mattana for useful comments. This research made use of data obtained from Data ARchives and Transmission System (DARTS), provided by Center for Science-satellite Operation and Data Archives (C-SODA) at ISAS/JAXA. P.E. acknowledges financial support from the Autonomous Region of Sardinia through a research grant under the programme PO Sardegna FSE 2007−2013, L.R. 7/2007 "Promoting scientific research and innovation technology in Sardinia". This research has made use of data obtained from the High Energy Astrophysics Science Archive Research Center (HEASARC) and the Leicester Database and Archive Service (LEDAS), provided by NASA's Goddard Space Flight Center and the Department of Physics and Astronomy, Leicester University, UK, respectively. S.R.O. acknowledges the support of the UK Space Agency.

References

Abdo, A. A., Ackermann, M., Atwood, W. B., et al. 2009a, ApJ, 695, L72
Abdo, A. A., Ackermann, M., Ajello, M., et al. 2009b, ApJS, 183, 46
Abdo, A. A., Ackermann, M., Ajello, M., et al. 2010a, ApJ, 720, 272
Abdo, A. A., Ackermann, M., Ajello, M., et al. 2010b, ApJS, 187, 460
Abramowski, A., Acero, F., Aharonian, F., et al. 2011, A&A, 525, A46
Ackermann, M., Ajello, M., Baldini, L., et al. 2011, ApJ, 726, 35
Appenzeller, I., Fricke, K., Fürtig, W., et al. 1998, The Messenger, 94, 1
Arnaud, K. A. 1996, Astronomical Data Analysis Software and Systems V, eds. G. H. Jacoby, & J. Barnes (San Francisco: ASP), 101, 17
Atwood, W. B., Abdo, A. A., Ackermann, M., et al. 2009, ApJ, 697, 1071
Bamba, A., Anada, T., Dotani, T., et al. 2010, ApJ, 719, L116
Bertin, E., Mellier, Y., Radovich, M., et al. 2002, in ADASS XI, ASP Conf. Ser., 281, 228
Bignami, G. F., & Caraveo, P. A. 1996, ARA&A, 34, 331
Breeveld, A. A., Curran, P. A., Hoversten, E. A., et al. 2010, MNRAS, 406, 1687
Breeveld, A. A., Landsman, W., Holland, S. T. et al., 2011, in GRB 2010 Symp., AIP Conf. Ser., in press [arXiv:1102.4717]
Burrows, D. N., Hill, J. E., Nousek, J. A., et al. 2005, SSRv, 120, 165
Cordes, J. M., & Lazio, T. J. W. 2002 [arXiv:astro-ph/0207156]
Durant, M., Kargaltsev, O., & Pavlov, G. G. 2011, ApJ, 743, 38
Fitzpatrick, E. L. 1999, PASP, 111, 63
Hobbs, G., Lorimer, D. R., Lyne, A. G., & Kramer, M. 2005, MNRAS, 360, 974
Kargaltsev, O., & Pavlov, G. G. 2010, in X-ray Astronomy 2009, AIP Conf. Proc., 1248, 25
Keith, M. J., Johnston, S., Kramer, M., et al. 2008, MNRAS, 389, 1881
Koyama, K., Tsunemi, H., Dotani, T., et al. 2007, PASJ, 59, 23
Krautter, J., Zickgraf, F.-J., Appenzeller, I., et al. 1999, A&A, 350, 743
Lasker, B. M., Lattanzi, M. G., McLean, B. J., et al. 2008, AJ, 136, 735
Lattanzi, M. G., Capetti, A., & Macchetto, F. D. 1997, A&A, 318, 997
Marelli, M., De Luca, A., & Caraveo, P. A. 2011, ApJ, 733, 82
Mignani, R. P. 2011, AdSpR, 47, 1281
Mignani, R. P., Sartori, A., De Luca, A., et al. 2010, A&A, 515, A110
Mignani, R. P., Shearer, A., De Luca, A., et al. 2011, A&A, 533, A101
Mitsuda, K., Bautz, M., Inoue, H., et al. 2007, PASJ, 59, 1
Newberry, M. V. 1991, PASP, 103, 122
Poole, T. S., Breeveld, A. A., Page, M. J., et al. 2008, MNRAS, 383, 627
Predehl, P., & Schmitt, J. H. M. M. 1995, A&A, 293, 889
Raymond, J. C., & Smith, B. W. 1977, ApJS, 35, 419
Roming, P. W. A., Kennedy, T. E., Mason, K. O., et al. 2005, Space Sci. Rev., 120, 95
Serlemitsos, P. J., Soong, Y., Chan, K.-W., et al. 2007, PASJ, 59, 9
Skrutskie, M. F., Cutri, R. M., Stiening, R., et al. 2006, AJ, 131, 1163
Smith, D. A., Guillemot, L., Camilo, F., et al. 2008, A&A, 492, 923
Sugizaki, M., Kamae, T., & Maeda, T. 2009, PASJ, 61, S55
Thompson, D. J. 2008, Rep. Prog. Phys., 71, 116901
Uchiyama, Y., Maeda, Y., Ebara, M., et al. 2008, PASJ, 60, 35
Weltevrede, P., Johnston, S., Manchester, R. N., et al. 2010, PASP, 27, 64
Zacharias, N., Finch, C., Girard, T., et al. 2010, AJ, 139, 2184
Zharikov, S. V., Shibanov, Yu. A., & Komarova, V. N. 2006, AdSpR, 37, 1979